Study of Ge-rich GeSbTe etching process with different halogen plasmas

Yann Canvel, Sébastien Lagrasta, Christelle Boixaderas, Sébastien Barnola, Yann Mazel, Eugénie Martinez

Study of Ge-rich GeSbTe etching process with different halogen plasmas

Yann Canvel, Sébastien Lagrasta, Christelle Boixaderas, Sébastien Barnola, Yann Mazel, and Eugénie Martinez

Citation: Journal of Vacuum Science & Technology A **37**, 031302 (2019); doi: 10.1116/1.5089037
View online: https://doi.org/10.1116/1.5089037
View Table of Contents: https://avs.scitation.org/toc/jva/37/3
Published by the American Vacuum Society

Study of Ge-rich GeSbTe etching process with different halogen plasmas

Yann Canvel,[1,a)] Sébastien Lagrasta,[1] Christelle Boixaderas,[2] Sébastien Barnola,[2] Yann Mazel,[2] and Eugénie Martinez[2]
[1]*STMicroelectronics, 850 rue Jean Monnet, 38926 Crolles, France*
[2]*CEA-LETI, University of Grenoble Alpes, 38000 Grenoble, France*

(Received 16 January 2019; accepted 18 March 2019; published 9 April 2019)

Chalcogenide materials based on GeSbTe (GST) ternary alloys are patterned using inductively coupled plasma in the manufacturing of phase change memories. The current process challenge is to maintain the GST composition and surface morphology to guarantee the memory performances. In this paper, the authors investigate the etching effects of different halogen plasmas (HBr, CF_4, and Cl_2) on an optimized Ge-rich GST alloy. Using x-ray photoelectron spectroscopy (XPS) and plasma profiling time-of-flight mass spectrometry as complementary techniques, the authors noticed that the etched GST surface shows a stronger Te-rich damaged layer in the sequence of $CF_4 > Cl_2 > HBr$. It is closely related to the higher affinity between halogen and GST elements in the sequence of Ge > Sb > Te. By comparing the etch rates with and without rf bias voltage, HBr etching is shown to be mainly related to the physical ion bombardment. On the contrary, Cl_2 plasma is mostly chemical and generates the roughest surface. The presence of a C-F passivation layer with CF_4 plasma shows that both chemical reactivity and physical bombardment are necessary to etch efficiently the GST film. The oxidation of the HBr-etched GST surface was monitored by XPS as a function of several air exposure times. As a conclusion, the GST oxidation becomes critical after 24 h of air exposure. *Published by the AVS.*
https://doi.org/10.1116/1.5089037

I. INTRODUCTION

Chalcogenide phase change materials, such as GeSbTe (GST) alloys, have shown outstanding properties, which have led to their successful use for a long time in optical memories such as digital video discs and, recently, in non-volatile resistive random access memories. The latter, known as phase change memories (PCMs), are among the most promising candidates to be integrated into next generation smart power and automotive applications.[1,2] Chalcogenide PCMs exhibit fast and reversible phase transformations between crystalline and amorphous structures with very different resistivity states. The amorphous phase is characterized by a high electrical resistivity while the crystalline phase has unambiguous lower resistivity. This distinctive ability to store the information gives a unique set of features for PCMs, such as fast programming, flexible scalability, high data retention, and performing endurance.[3,4]

The material properties, for example, the crystallization temperature, may be tuned considerably by changing the concentration of one element (Ge, Sb, or Te) with a huge potential impact on the memory performances. For instance, Cheng *et al.*[5] reported an increase in the crystallization temperature by adding Ge to the material. They mentioned the particular "golden composition" corresponding to a Ge-rich $Ge_2Sb_1Te_2$ alloy which improves the thermal stability of the memory. An accurate control of the GST composition is needed in order to reach the performances required for their integration in electronic devices. In our study, we investigate an optimized Ge-rich GST alloy to meet with the industrial requirements in terms of PCMs' thermal stability.

GeSbTe based materials are known to be easily disturbed and damaged when exposed to reactive atmospheres.[6–13] In the perspective of large-scale integration, which means incorporation of the PCM into more and more confined structures, the device performances are getting increasingly more sensitive to surface effects of the GST layer. Thus, it is crucial to maintain a homogeneous composition in the GST surface/volume all along the manufacturing process, especially during the etching process. Kang *et al.* and other groups[6–9] have studied the etch damage of the standard $Ge_2Sb_2Te_5$ induced by different halogen-based plasmas. They have shown that HBr plasma induces lower damages than other plasmas. However, the potential impact of plasma etching may change with the GST composition and nothing is known regarding a Ge-rich GST alloy.

In this article, a complete study of the etching of the optimized Ge-rich GST alloy is performed. The potential damages induced by three halogen gases (such as HBr, CF_4, and Cl_2) used in inductively coupled plasma (ICP) are highlighted thanks to several complementary techniques of material characterization. More specifically, the etching effect of GST with these three halogen gases is investigated using x-ray photoelectron spectroscopy (XPS) to monitor chemical surfaces changes. A complementary technique, the plasma profiling time-of-flight mass spectrometry (PP-TOFMS), is also used to get information about in-depth elemental distributions. The etch mechanisms and kinetics implemented by these halogen plasmas are also described. Finally, we focus on the GST oxidation dynamics occurring after the HBr etching process, when exposed to air.

II. EXPERIMENTAL METHODS

100-nm-thick GST films were deposited on 12 in. SiN/SiO_2/Si substrates by rf magnetron co-sputtering (AMAT Endura 300B). Note that throughout the paper, the so-called

[a)]Electronic mail: yann.canvel@st.com or yann.canvel@cea.fr

Ge-rich GST is not the stoichiometric $Ge_2Sb_2Te_5$ alloy but a GST doped with an optimized percentage of Ge, in excess compared to Sb and Te.

The etching process was performed in a 12 in. planar ICP reactor (Lam Research, 2300 Kiyo CX). A 13.56 MHz rf TCP and bias power were generated to produce high density plasma and accelerating voltage near the sample. The etching parameters of rf source power, rf bias voltage, and chamber pressure were set at 770 W, 205 V, and 3 mTorr, respectively. The temperature of the sample holder was controlled by a helium injection system and fixed at 30 °C. Lastly, the flow of halogen gas was maintained at 100 sccm without any dilution.

The GST etching was monitored by optical emission spectrometry (OES, Lam Versys 2300). The GST thickness remaining after partial etching was measured by x-ray reflectometry (Jordan Valley 5200T). The surface morphology and roughness were examined using scanning electron microscopy (SEM, Hitachi S5500) and atomic force microscopy (AFM, Bruker Dimension Fastscan), respectively. The chemical composition and the corresponding quantification of the etched GST surface were evaluated by XPS. The Thermo Fisher Scientific Theta 300 tool equipped with a monochromatic Al Kα line X-ray source at 1486.7 eV was used. This instrument is equipped with a specific lens and a two-dimensional detector allowing a parallel acquisition of photoelectrons emitted from 20° to 80° emission angles. For all XPS spectra shown in this paper, the intensity is obtained by adding the signal measured over the whole angular range of the detector, except when the angles are specified. Quantification of the chemical composition was done by normalizing the peak areas, integrated over the whole spectral range, with relative sensitivity factors provided by the tool manufacturer. Samples were transferred from the ICP reactor to the XPS tool with an Adixen vacuum carrier under primary vacuum. In addition, PP-TOFMS was performed to provide the in-depth chemical composition of the GST material. PP-TOFMS is a recent technique developed by Horiba, combining an argon plasma for sample sputtering and ionization with a time-of-flight mass spectrometer for identifying the ionized species.[14] The technique provides fast calibration free semiquantitative analysis (few nm/s) while inducing low surface damage (50 eV sputtering kinetic energy). Semiquantification is achieved by simply rationing the ionic currents, via the Ion Beam Ratio method.[15,16] Results are presented as a function of depth which is determined from the sputtering rate of the material.

III. RESULTS AND DISCUSSION

A. Etching effects of halogen-based plasmas on Ge-rich GST

Here, the experimental protocol consists of etching partially the GST layer deposited on a blanket wafer with HBr, CF_4, and Cl_2 plasmas. The etch depth of GST was maintained at about 40 nm. Then, the etched GST surface is characterized using several complementary techniques.

Figure 1 shows the XPS spectra of Ge, Sb, and Te obtained by quasi *in situ* analyses of Ge $2p_{3/2}$, Sb $3d_{5/2}$, and Te $3d_{5/2}$ core level peaks, more sensitive to the surface environment. Note that we refer to measurements done using a vacuum carrier to avoid air exposure between plasma etching and XPS analysis as quasi *in situ* analyses. The GST chemical environment is clearly identified for each element and respectively located at 1218.1 eV [Ge(GST)], 528.7 eV [Sb(GST)], and 573.1 eV [Te(GST)]. In the case of the HBr

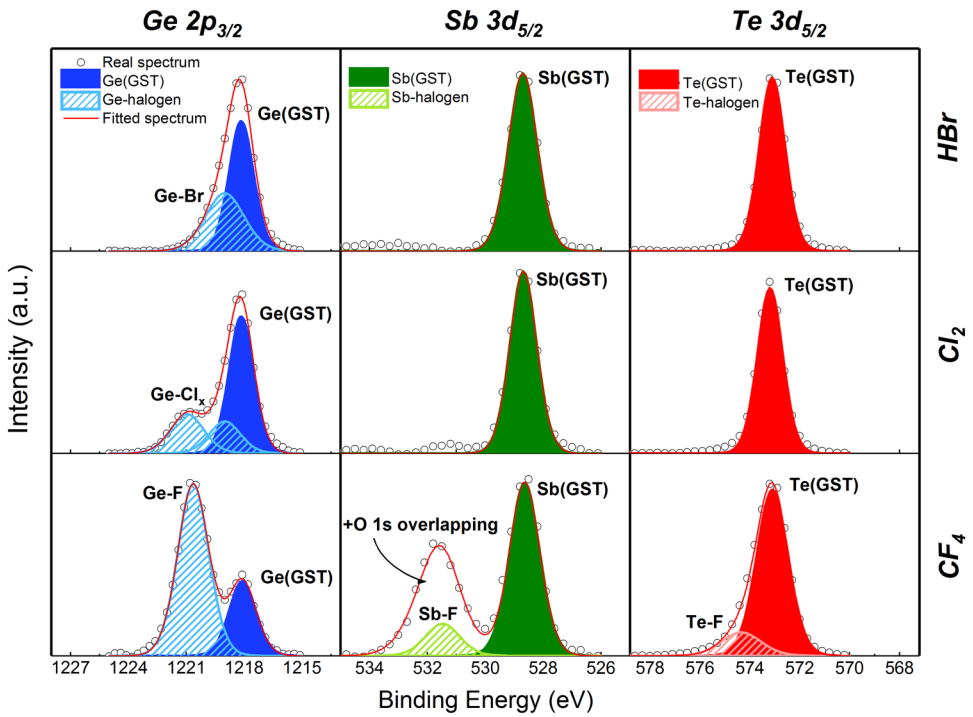

FIG. 1. XPS spectra of Ge, Sb, and Te elements after the GST partial etching in HBr, Cl_2, and CF_4 plasmas.

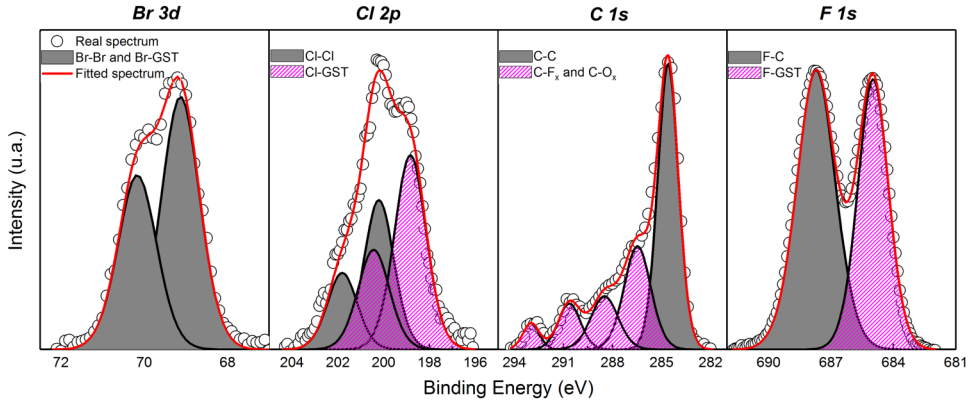

FIG. 2. XPS spectra of Br, Cl, and F elements after the GST partial etching in HBr, Cl_2, and CF_4 plasmas together with the carbon spectrum measured after CF_4 plasma etching of GST.

plasma, only Ge is slightly connected to Br-atoms with the presence of halide bonding at 1219 eV. The GST environment of Sb and Te remains stable. In comparison, the Cl_2 plasma shows higher reactivity with Ge atoms. Both halogenated peaks, at 1219.0 and 1220.9 eV, stand for the strong Ge–Cl_x bindings.[6,7] For the CF_4 plasma, the halogenation is much more intense. The Ge-F_x peak at 1220.6 eV is dominant compared to the Ge(GST) peak whose intensity sharply decreased. Unlike the case of HBr and Cl_2 plasmas, Sb and Te elements are also bonded to the incorporated halogen atoms. Indeed, Sb-F_x and Te-F_x halide peaks are observed at 531.2 eV and 574.3 eV, respectively. Note that we observe an oxygen contamination with the presence of O 1s peak at 531.7 eV, which overlaps with the Sb $3d_{5/2}$ peak after the CF_4 etching process, due to a possible oxygen contamination from the ICP reactor walls during plasma etching. The Sb-F_x contribution has been extracted taking the Sb-F_x/Sb-GST area ratio measured for the Sb $3d_{3/2}$ peak.

The Br 3d, Cl 2p, and F 1s spectra measured with the three halogen plasmas are also presented in Fig. 2. Only one doublet is identified for the Br 3d spectrum (Br $3d_{5/2}$ at 69.1 eV), assigned to both Br-Br and Br-GST chemical environments. Two contributions are extracted for the Cl 2p peak, respectively, related to Cl–Cl (Cl $2p_{3/2}$ at 200.2 eV) and Cl–GST (Cl $2p_{3/2}$ at 198.8 eV) bonds. The C 1s peak highlights one main contribution assigned to hydrocarbon contamination together with four contributions related to C–O_x and C–F_x bonds. The C–F_x bonds are also clearly identified on the F 1s peak (687.7 eV) together with the F–GST bonding states (685.0 eV).

The GST chemical environment is clearly disturbed by the formation of GST halides (halogenated GST) during plasma etching. XPS spectra indicate the incorporation of halogens inside the GST, yielding direct bonding with GST elements. The reactivity between the halogens and GST elements is higher in the sequence of F > Cl > Br, as shown by the formation of Ge–F, Sb–F, and Te–F bonds for CF_4 whereas only Ge–Br (resp., Ge–Cl) can be detected for HBr (resp., Cl_2). This trend is confirmed by comparing the strength of the chemical bonds in diatomic molecules (kJ/mol) for Ge and Sb halides (no data available for Te):[17]

$$\mathrm{F{-}Ge}\ (485 \pm 21) > \mathrm{Cl{-}Ge}\ (\sim 431) > \mathrm{Ge{-}Te}\ (340 \pm 14.6) > \mathrm{Br{-}Ge}\ (255 \pm 29),$$

$$\mathrm{F{-}Sb}\ (439 \pm 96) > \mathrm{Cl{-}Sb}\ (360 \pm 50) > \mathrm{Br{-}Sb}\ (314 \pm 59) > \mathrm{Sb{-}Te}\ (299.2 \pm 6.3).$$

To further evaluate the effect of the halogen-based plasma etching, XPS quantification was carried out in the etched GST layer and the results are gathered in Table I. The atomic percentages of the corresponding halogen content are mentioned in the first line of the table (at. % of Br, Cl, and F). They were obtained using the total area of the Br 3d, Cl 2p, and F 1s spectra shown in Fig. 2. A higher F content (35 at. %) is measured compared to Cl (11 at. %) and Br (5 at. %), confirming the higher reactivity of CF_4 plasma mentioned in the previous paragraph. Note that the F atomic concentration might be overestimated because of the smaller probed depth of F 1s (~4 nm at 45°) compared to the GST core levels (~6 nm at 45°).[17] An estimation of the residual oxygen at the GST surface is given in the second line. No oxygen is seen on the GST surface after HBr and Cl_2 plasmas (<1 at. % which is the XPS sensitivity), as shown by the Sb $3d_{5/2}$ spectra in Fig. 1 where no O1s signal is seen. A small oxygen content (5 at. %) is measured after the CF_4

TABLE I. Relative atomic concentration (at. %), given with 20% of uncertainty, of the halogen (Br, Cl, and F) and oxygen measured by XPS at the GST surface and ratios between element concentration (Ge, Sb, and Te) measured after and before plasma etching.

Halogen plasma	HBr	Cl_2	CF_4
At. % halogen	5 (±1)	11 (±2)	35 (±7)
At. % oxygen	<1	<1	5 (±1)
Ge_{exp}/Ge_{ref}	0.95	0.83	0.59
Sb_{exp}/Sb_{ref}	0.79	0.77	0.42
Te_{exp}/Te_{ref}	1.26	1.58	2.45

plasma etching, due to a possible contamination from the ICP chamber walls.

Below, the halogen contents were extracted from the total area of Ge 3d (30 eV), Sb 4d (33 eV), and Te 4d (40 eV) core levels, all located at low binding energies. Indeed, the use of the previous Ge $2p_{3/2}$, Sb $3d_{3/2}$, and Te $3d_{5/2}$ peaks is not possible for quantification, the Ge $2p_{3/2}$ peak being too far from the other core levels. Note that, using the Ge 3d, Sb 4d, and Te 4d set of core levels, the volume versus surface contribution is higher compared to the previous core levels. This is due to a larger probed depth,[17] equal to 6 nm for the three elements at 45° compared to 2 nm for Ge $2p_{3/2}$ and 4 nm for Sb $3d_{3/2}$ and Te $3d_{5/2}$.The values given in Table I correspond to the ratios between the element concentration after the partial etching (e.g., Ge_{exp}) of GST and the as-deposited one (e.g., Ge_{ref}). As previously, the wafer transfer from the etching cluster to the XPS tool was executed without air exposure to avoid the oxidation of the GST surface which is likely to prevent any XPS quantification. Indeed, quantifying the stoichiometry of oxidized GST is very difficult because of the overlap between Ge oxides (~32 eV) and Sb from GST (33 eV). The XPS quantification was done assuming a homogeneous GST composition. However, PP-TOFMS results presented later show the presence of a surface layer whose composition differs from the bulk GST. Due to this gradient, the relative atomic concentrations are thus given with 20% of uncertainty.

In the case of HBr plasma, the contamination is pretty low with only 5 at. % of Br incorporation into the GST matrix. The different element ratios, especially the Ge ratio, are relatively close to unity. It means that the modification of the Ge-rich GST composition induced by the etching plasma is limited. However, we can notice inverted evolutions of Sb and Te ratios resulting in an increase in the Te concentration in the GST top layer. For the Cl_2 plasma, the higher reactivity between chlorine and GST is confirmed by the presence of 11 at. % halogen content. Besides, the formation of a Te-rich phase with the increase in Te ratio is even more remarkable. Lastly, the CF_4 plasma etching induces the worst effect on the GST composition. A high fluorine content is measured (35 at. %), from which F–GST and C–F_x contributions correspond to 16 and 19 at. %, respectively. This result shows the implantation of fluorine in the GST as well as the formation of a C-F-rich layer above the GST surface. This is confirmed when comparing the F 1s spectra measured at 23° and 76° emission angles (not shown). An increase in the C–F_x contribution, from 46% to 68% of the total F1s area, is observed when going from a bulk (23°) to a surface (76°) analysis. In addition, the Ge and Sb ratios collapse while the Te ratio sharply increases. Consequently, the initial Ge-rich GST composition is completely lost and the formation of a C-F-rich surface layer together with an underlying strong Te-rich phase is promoted in the etched GST film.

To appreciate how deep the GST composition is modified by the etching plasma, Fig. 3 shows the PP-TOFMS profiles measured for the three etched GST. The results provide in-depth elemental compositions which are complementary with the previous XPS surface analyses. They confirm the formation of a Te-rich phase when approaching the GST surface for the three halogen plasmas. This degradation is confined at the extreme surface for HBr-etched GST (<2 nm). As already shown by XPS, the CF_4 etching induces a critical chemical modification resulting here in a deeply modified GST profile. The Ge-rich GST composition is only found after 6 nm of probed material. As already noticed, the Cl_2 plasma has an intermediate effect between the two others.

The systematic Ge loss is actually related to the high reactivity of Ge atoms with halogen gases. As shown by XPS, halogens react preferentially with Ge forming Ge–Br, Ge–Cl, and Ge–F bonds, whereas the chemical environment of Te and Sb remains more stable. The Ge depletion can also be explained by considering the very different volatilities of Ge, Sb, and Te halides. The boiling points of halogen compounds of Ge, Sb, and Te are given in Table II at standard temperature and pressure, which defines the degrees of volatility of potential GST halides.[18]

On the whole, GST halides are more volatile in the element sequence of Ge > Sb > Te and the halogen gas sequence of F > Cl > Br. As a consequence, Ge atoms will be systematically vaporized in priority during the etching process, yielding a Ge-poor phase (equivalent to a Te-rich phase). And this degradation will be the most intense in the presence of fluorine gas because its high reactivity with Ge elements will generate much more volatile by-products. Note that, given the high

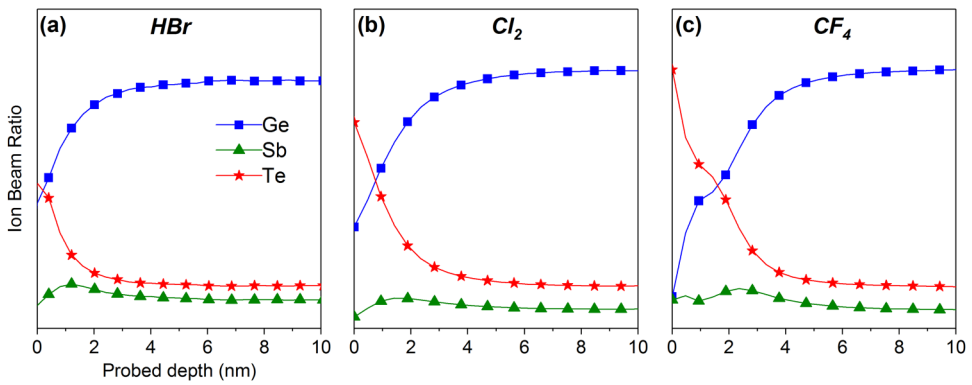

FIG. 3. GST depth profiles obtained using PP-TOFMS after the GST partial etching in (a) HBr, (b) Cl_2, and (c) CF_4 plasmas.

TABLE II. Boiling points of halogen compounds of Ge, Sb, and Te.

	Ge		Sb		Te	
	Bonding	b.p. (°C)	Bonding	b.p. (°C)	Bonding	b.p. (°C)
F	GeF_4	−36.5	SbF_5	141	TeF_4	196
	GeF_2	130	SbF_3	345	TeF_6	−39
Cl	$GeCl_4$	86.6	$SbCl_3$	220	$TeCl_2$	328
	$GeCl_2$	↑	$SbCl_5$	140	$[TeCl_4]_4$	387
Br	$GeBr_4$	186	$SbBr_3$	286	$TeBr_2$	339
	$GeBr_2$	150			$[TeBr_4]_4$	414

volatility of TeF_6 and GeF_4 species, one would expect the formation of an Sb-rich rather than a Te-rich phase at the GST surface. This is however very unlikely because of the very small Sb content in the initial GST composition.

To complete this study, SEM and AFM images of the etched GST surfaces are shown in Fig. 4. In addition, the root mean square surface roughness has been determined for each case (0.87 nm for HBr, 6.32 nm for Cl_2, 1.10 nm for CF_4). From this comparison, the Cl_2 etched surface is clearly identified as the roughest one. It may be caused by the high reactivity with GST and the formation of nonvolatile by-products. In an opposite case, HBr plasma generates the smoothest etched surface despite the presence of corrosion pits, owing to the unique formation of nonvolatile Ge–Br complexes. For the CF_4 plasma, the fluorine and carbon interaction with the GST is sufficiently important to form a C-F protecting layer which limits further surface damages induced by the reactive plasma. To conclude, the HBr-etched sample offers the lowest surface roughness, which perfectly matches with the previous XPS and PP-TOFMS results showing the lowest chemical modifications of the GST surface/volume.

To summarize this first part, we have evaluated how the interaction of halogen plasmas with GST is likely to damage its surface and bulk stoichiometry. More particularly, we focused on the modification of the Ge-rich GST composition induced by three kinds of halogen-based plasmas. XPS analyses provided the relative degree of reactivity between halogen and GST elements through their ability to halogenate the material. The PP-TOFMS profiles confirmed the specific evolution of Ge, Sb, and Te contents as a function of depth. Finally, the microscopy observations allowed us to compare the GST surface morphology after the different etching processes. As a result, the HBr plasma can be considered as the best etching chemistry to minimize the degradation of the Ge-rich GST composition, the halogen contamination and the surface roughness. It is mainly related to the relatively low reactivity of Br with GST elements amongst studied halogens.

B. Etching kinetics and mechanisms

In this part, we investigate the etching kinetics of the halogen-based plasmas by comparing the etch rates measured using *in situ* OES. The GST etch rate can be directly approximated by following the intensity of the Ge signal during the etching step. The Ge optical emission was collected by optical fiber at a wavelength of 265 nm, and monitored as a function of etching time. For the three plasmas (see Fig. 5), it was found that the Ge signal rose gradually and began to drop after it reached its maximum intensity point. The rising region corresponds to the increase in the concentration of the volatile Ge halides generated during the efficient GST etching. Then, when the GST layer is almost entirely removed, the Ge intensity decreases sharply until it stabilizes indicating the end of the GST etching. Note that, regarding the CF_4 plasma etching, the intensity rise when etching is started as well as the high residual intensity after GST removal are probably due to interferences with optical emission from CF_2 radicals[18] ($\lambda = 262.9$ and 271.1 nm).

From these curves, the GST etch rate for the three halogen plasmas is found to be 192 nm/min for HBr, 714 nm/min for Cl_2, and 163 nm/min for CF_4. Similar measurements were

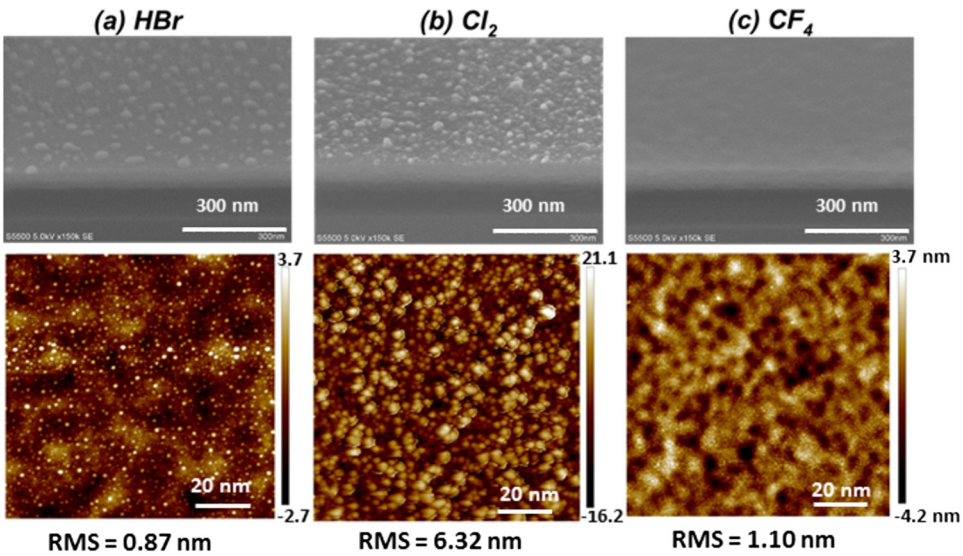

FIG. 4. SEM images of tilted view and AFM images for the GST films etched by (a) HBr, (b) Cl_2, and (c) CF_4 plasmas.

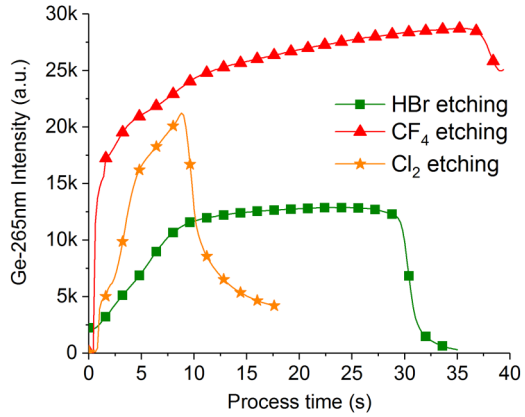

FIG. 5. Signal intensity variations of Ge during the GST etching in HBr, Cl_2, and CF_4 plasmas.

done without any rf bias voltage applied on the sample. This voltage is used to boost the ion bombardment during the GST etching process. When switched off, only chemical reactions forming volatile species induce some GST etching. All the related results have been gathered in Table III.

In the case of the HBr plasma, the low chemical reactivity of Br with GST elements leads to the drop of the etch rate when the bias is turned off. Only the physical ion bombardment, tuned by the applied rf bias voltage contributes to an efficient GST etching. In an opposite case, the GST etching with the Cl_2 plasma is mostly chemical because the application of a rf bias voltage has no significant effect on the GST etch rate. It mainly correlates with the strong chemical affinity between Cl and Ge, as shown in Sec. III A. For the CF_4 plasma, the etch rate falls down without bias. The formation of a thick C-F polymer on the GST layer is even more promoted when no anisotropic and physical bombardment contributes to its limited growth. This is confirmed by a careful analysis of the F 1s spectrum (not shown): 96% of the total area corresponds to the $C–F_x$ contribution, whereas the F–GST is nearly not detected (4% of the total area). Without bias, the extreme incorporation of carbon limits the diffusion of reactive F-radicals to the active GST surface and, consequently, lowers drastically the GST etch rate.[10,11]

These results confirm that the interaction of halogen chemistries with the GST material can be very different: HBr etching is mainly physical, whereas Cl_2 etching is mostly chemical. Regarding CF_4, both chemical reactions and ion bombardment play a critical role. An efficient etching is obtained by combining the high chemical reactivity of fluorine with GST with physical bombardment of the C-F polymer formed at the surface. Therefore, the GST etching process can be adapted according to the technical specifications.

TABLE III. Etch rates of GST material for HBr, Cl_2, and CF_4 plasmas with/without rf bias voltage.

Halogen plasma	HBr	Cl_2	CF_4
Etch rate (nm/min) with bias	192	714	163
Etch rate (nm/min) without bias	~60	627	~98

C. Oxidation dynamics of the etched GST surface

In a standard microelectronic manufacturing process, the etching step is commonly followed by some unavoidable air break and queue time, occurring between tool transfers in particular. It may induce partial oxidation of the GST material and have a negative effect on the phase change memories properties. Yashina *et al.*[12] have investigated the oxidation steps of GeTe surfaces after the deposition process. Gourvest *et al.*[13] completed this study by analyzing the impact of oxidation on GeTe and $Ge_2Sb_2Te_5$ materials' properties. Firstly, the oxygen atoms diffuse into the GST matrix, yielding a preferential formation and the growth of germanium and antimony oxides. This can be explained by comparing the enthalpy of formation between the potential oxides: $\Delta H^0 = -709.7$ kJ/mol for Sb_2O_3, $\Delta H^0 = -580$ kJ/mol for GeO_2, and $\Delta H^0 = -322$ kJ/mol for TeO_2.[18,19] This mechanism is accompanied by the increase in nonoxidized Te and thus the formation of a Te-rich phase at the surface. The oxidation is enhanced during long exposure times. After 30 days of air exposure, this process is characterized by the presence of a mixture of tellurium and germanium oxides at the extreme surface of the material. The incorporation of oxygen modifies the stoichiometry of the initial fresh GST material, giving rise to the reduction of its crystallization temperature T_c. As a consequence, the thermal stability of the phase change material could be degraded. In this work, the oxidation dynamics are studied just after the etching process when the phase change material is not covered anymore and, potentially, exposed to air. To do so, we partially etch the GST material with halogen plasmas and analyze the evolution of the surface layer composition after several air exposure durations in a clean room atmosphere. In light of our previous results (cf. Secs. III A and III B), it was found that HBr chemistry promotes the least invasive etching of the Ge-rich GST material. Therefore, it is more appropriate to investigate the aging of GST after HBr plasma etching.

Table IV shows the evolution of O, C, and Br concentrations into the GST matrix according to various air exposure times. These values were extracted from the total area collected over the 20°–80° angular range of O 1s (532.8 eV), C 1s (284.8 eV), and Br $3d_{5/2}$ (69.1 eV) core levels.

During the first hours, the etched GST surface is weakly contaminated with only 2 at. % of oxygen and carbon contents. The incorporation of Br comes from the Br-based plasma used to etch partially the GST layer. Within a few days, we observe a progressive GST oxidation accounting for a 20 at. % O concentration increase after 5 days of aging. On the other hand, Br

TABLE IV. Relative atomic concentrations (at. %), given with 20% uncertainty, of the contaminants (O, C, and Br) measured by XPS at the GST surface after HBr-based plasma etching.

Air exposure time	4 h	24 h	5 d	30 d	90 d
At. % O	2 (±0.4)	3 (±0.6)	20 (±4)	53 (±11)	51 (±10)
At. % C	2 (±0.4)	4 (±0.8)	5 (±1)	12 (±2)	13 (±0.3)
At. % Br	6 (±1)	3 (±0.6)	1 (±0.2)	<1	—

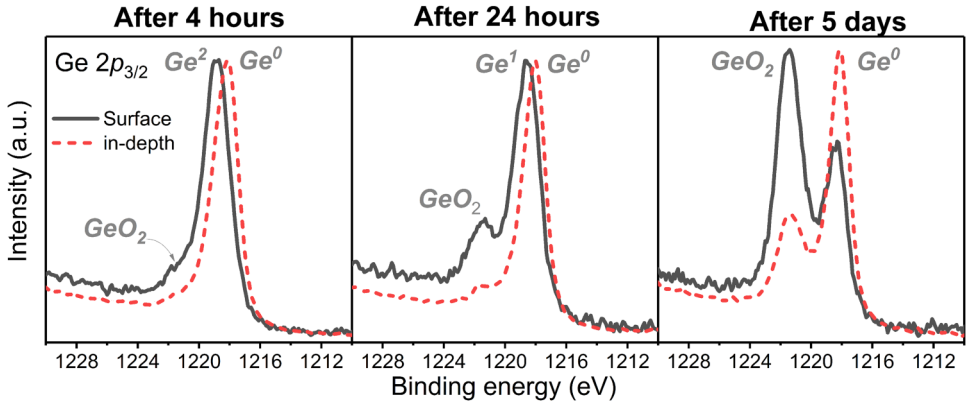

FIG. 6. Angle-resolved XPS spectra of Ge $2p_{3/2}$ measured at 76° and 23° emission angles for different air exposure times after the GST partial etching in HBr plasma.

concentration drops with exposure time while the carbon contamination is increasingly more present at the surface. After 30 days of air exposure, the oxygen and carbon concentrations seem to reach a saturation point with a little more than 50 at. % and 10 at. %, respectively, at the GST surface. All Br content, initially generated during the etching process, has disappeared. This opposite evolution between the halogen and the oxygen concentrations is consistent with the changes observed on the Ge $2p_{3/2}$ spectra (see Fig. 6). Here, the overlayer of etched GST was probed by angle-resolved XPS with increasing exposure times (4 h, 24 h, and 5 days). Two Ge spectra can be extracted at 76° (solid line) and 23° (dotted line) emission angles, one more sensitive to the surface environment and the other more sensitive to the in-depth environment.

In the case of 4 h air exposure, the surface spectrum is shifted with respect to the in-depth one. Indeed, the Ge peak typical from GST located at 1218.1 eV (Ge^0) turns into the halide bonding Ge–Br at 1219 eV (Ge^2) when being more surface sensitive. It is related to the surface halogenation generated during the HBr plasma etching of the GST layer. As already noticed in Table IV with the oxygen quantification, the GST oxidation occurs at the extreme surface with the emergence of GeO_2 at 1221.4 eV. After 24 h of aging, the decrease of Br content tends to weaken the halide bonding which is illustrated by the shift of the surface spectra toward the GST environment, at 1218.5 eV (Ge^1). At the same time, the oxygen incorporation into the GST material is more important and the oxide peak is growing for both spectra.

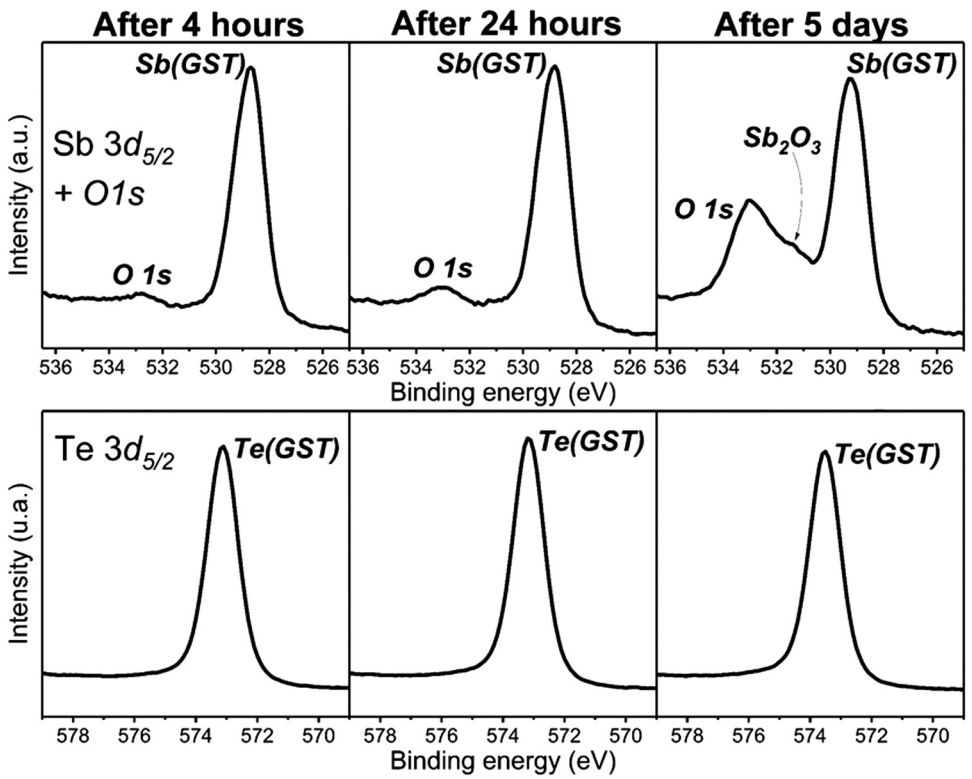

FIG. 7. XPS spectra of Sb $3d_{5/2}$ and Te $3d_{5/2}$ measured for different air exposure times after the GST partial etching in HBr plasma.

Finally, after 5 days, the halogen contamination is almost negligible since both spectra are lined up. At the surface, Ge atoms are mostly bonded to oxygen as shown by the predominant GeO_2 contribution. When being more depth sensitive, the Ge–GST bonds remain in majority but the diffusion of oxygen atoms into the GST volume is noteworthy with the rising presence of the oxide peak in the in-depth spectrum.

The Sb $3d_{5/2}$ and the Te $3d_{5/2}$ spectra measured with increasing exposure times (4 h, 24 h, and 5 days) are also presented in Fig. 7. The Sb $3d_{5/2}$ spectra show an increasing Sb oxidation with air exposure together with a consistent increase in the O 1s neighboring spectra. This is highlighted by the Sb_2O_3 contribution rising near the main Sb-GST peak after 5 days of air exposure. On the opposite, Te remains more stable with no change observed on the Te $3d_{5/2}$ spectra. These results show the preferential oxidation of germanium and antimony with respect to tellurium during aging of GST.

These results allow to understand how the contamination, generated during the etching process and the consecutive air exposure, is likely to modify the GST chemical environment. In addition, this modification was also investigated by monitoring the in-depth profiles of the GST elements in the same experimental conditions using PP-TOFMS, as shown in Fig. 8. The in-depth profiles of the etched GST layer are plotted after 4 h, 24 h, and 5 days of air exposure, respectively. Here, the most remarkable etching effect is the formation of a Te-rich phase at the extreme surface. For that matter, the GST profile obtained after 4 h air exposure is almost the same as the one obtained a few minutes after the etching process [represented in Fig. 3(a)]. The situation is getting worse when the GST material is exposed longer to the air. Indeed, after 1 or 5 days, the Te-rich phase becomes increasingly more substantial to the detriment of the Ge-rich bulk composition. This drift can be explained by the preferential formation of germanium and antimony oxides while tellurium atoms remain nonoxidized within the proposed time scale, as shown previously by XPS. Germanium oxides are known to be thermodynamically unstable and thus rather volatile,[20] yielding to a possible desorption during air aging. The lower affinity of Te with oxygen, resulting in the relative increase in the surface Te content with aging time, is consistent with the strength of chemical bonds decreasing from 659 kJ/mol for the diatomic molecule Ge-O to 434 kJ/mol for Sb-O and to 376 kJ/mol for Te-O.[18]

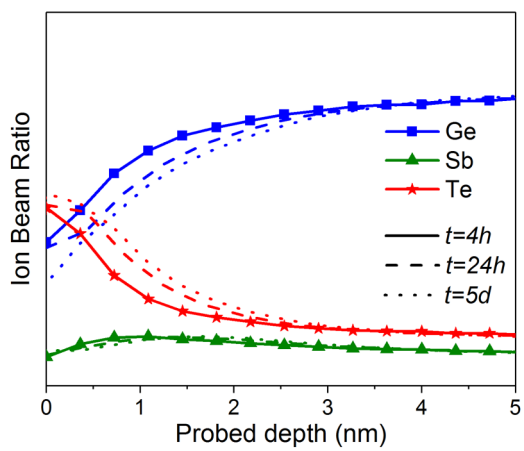

FIG. 8. GST depth profiles obtained using PP-TOFMS for different air exposure times after the GST partial etching in HBr plasma.

After the etching process, the uncovered GST surface is gradually oxidized. The strong affinity between Br and Ge is likely to delay the oxygen incorporation into the GST matrix within the first hours of air exposure. However, after 24 h of aging, the oxidation dynamics become critical. The GST surface tends to be Te-rich and the oxygen diffuses progressively in the depth of the material, as shown by the increasing O content measured by XPS. The same trend can be also observed on a GST surface after being etched by CF_4 and Cl_2 plasmas (not shown here). In any case, the loss of the Ge-rich GST composition could potentially alter the material properties like T_c and, more generally, the memory performances.[5,21,22]

IV. CONCLUSIONS

An optimized Ge-rich GST alloy is currently studied for phase change memories with improved performances such as better thermal stability. The effect of halogen-based plasma etching on this Ge-rich GST has been investigated by comparing various gases such as HBr, Cl_2, and CF_4. XPS results show the incorporation of halogens yielding to the formation of GST halides at the surface, with decreasing reactivity following the sequence $CF_4 > Cl_2 > HBr$. Moreover, the GST stoichiometry is strongly modified with the formation of a Te-rich phase at the surface in the case of CF_4, whereas modifications are rather limited with HBr, the Cl_2 having an intermediate impact. This Te-rich phase can be explained by the higher volatility of GST halides in the following sequence Ge > Sb > Te. Complementary PP-TOFMS and AFM measurements confirm that HBr offers the thinnest modified surface layer and the lowest surface roughness, thus being the most promising candidate to minimize the degradation of the Ge-rich GST surface composition and morphology.

By comparing the etch rates with and without rf bias voltage on the sample, the interaction of these gases with the GST surface was found to be mainly physical for HBr whereas it is mostly chemical for Cl_2, in agreement with a higher affinity between Cl and Ge. Regarding CF_4, the etching is probably related to the high chemical reactivity of fluorine with GST together with some physical bombardment of the C-F polymer formed at the surface.

Air exposure is unavoidable during the manufacturing process of phase change memories. We have thus investigated the aging of the etched GST surface, using the HBr plasma which is the least invasive process. XPS results have shown some preferential oxidation of Ge and Sb, compared to Te which remains more stable, thus enhancing the formation of a Te-rich phase at the GST surface. This oxidation starts to become critical after one day of air exposure.

ACKNOWLEDGMENTS

This study was performed in the context of the STMicroelectronics-CEA LETI collaboration. This work was supported by the French National Research Agency (ANR)

within the equipped IMPACT program, under Contract No. ANR-10-EQPX-33.

[1]M. Pasotti *et al.*, *43rd Proceedings of the ESSCIRC 2017*, Leuven, Belgium, September 2017 (IEEE, 2017), pp. 320–323.
[2]M. Pasotti *et al.*, IEEE J. Solid State Circuits **1**, 1 (2018).
[3]G. W. Burr *et al.*, J. Vac. Sci. Technol. B **28**, 223 (2010).
[4]W.-C. Chien *et al.*, *IEEE Trans. Electron Devices.*, November 2018, Vol. 65, No. 11, pp. 5172–5179.
[5]H. Y. Cheng *et al.*, *Proceedings of the IEDM*, Washington, DC, December 2011 (IEEE 2011), pp. 3.4.1–3.4.4.
[6]S.-K. Kang, M.-H. Jeon, J.-Y. Park, M. S. Jhon, and G.-Y. Yeom, Jpn. J. Appl. Phys. **50**, 086501 (2011).
[7]S.-K. Kang, M. H. Jeon, J. Y. Park, G. Y. Yeom, M. S. Jhon, B. W. Koo, and Y. W. Kim, J. Electrochem. Soc. **158**, H768 (2011).
[8]J. Li *et al.*, Appl. Surf. Sci. **378**, 163 (2016).
[9]Y. Song, R. Huang, Y. Zhang, and H. Zhang, *Proceedings of the CSTIC*, Shanghai, China, March 2016 (IEEE, 2016), pp. 1–3.
[10]L. Shen *et al.*, Appl. Phys. A **122**, 1 (2016).
[11]S.-K. Kang, J. S. Oh, B. J. Park, S. W. Kim, J. T. Lim, G. Y. Yeom, C. J. Kang, and G. J. Min, Appl. Phys. Lett. **93**, 043126 (2008).
[12]L. V. Yashina, R. Püttner, V. S. Neudachina, T. S. Zyubina, V. I. Shtanov, and M. V. Poygin, J. Appl. Phys. **103**, 094909 (2008).
[13]E. Gourvest, B. Pelissier, C. Vallée, A. Roule, S. Lhostis, and S. Maitrejean, J. Electrochem. Soc. **159**, H373 (2012).
[14]A. Tempez, S. Legendre, J.-P. Barnes, and E. Nolot, J. Vac. Sci. Technol. B **34**, 03H120 (2016).
[15]F. L. King, J. Teng, and R. E. Steiner, J. Mass. Spectrom. **30**, 1061 (1995).
[16]S. W. Schmitt, C. Venzago, B. Hoffmann, V. Sivakov, T. Hofmann, J. Michler, S. Christiansen, and G. Gamez, Prog. Photovoltaics Res. Appl. **22**, 371 (2014).
[17]QUASES software, see: http://www.quases.com/products/quases-imfp-tpp2m/ using the TTP-2M formula from S. Tanuma, C. J. Powell, and D. R. Penn, Surf. Interface Anal. **20**, 77 (1993).
[18]D. R. Lide, *CRC Handbook of Chemistry and Physics* (CRC, Boca Raton, 1995).
[19]M. Aspiala, D. Sukhomlinov, and P. Taskinen, Solid State Ion. **265**, 80 (2013).
[20]B. Onsia *et al.*, Solid State Phenom. **103–104**, 19 (2005).
[21]V. Sousa *et al.*, *VLSI Technology* (IEEE, 2015), pp. T98–T99.
[22]P. Noé, C. Vallée, F. Hippert, F. Fillot, and J.-Y. Raty, Semicond. Sci. Tech. **33**, 013002 (2018).